A mutation designed to alter crystal packing permits structural analysis of a tight-binding fluorescein–scFv complex

ANNEMARIE HONEGGER,[1] SILVIA SPINELLI,[2] CHRISTIAN CAMBILLAU,[2] AND ANDREAS PLÜCKTHUN[1]

[1]Biochemisches Institut der Universität Zürich, CH-8057 Zürich, Switzerland
[2]Architecture et Fonction des Macromolécules Biologiques, UPR 9039-CNRS, F-13402 Marseille Cedex 20, France

(Received April 17, 2005; Final Revision July 15, 2005; Accepted July 20, 2005)

Abstract

The structure of the scFv fragment FITC-E2, obtained from a naive phage antibody scFv library derived from human donors, was determined at 2.1 Å resolution in the free form and at 3.0 Å in the complexed form. The wild-type (wt) scFv binds fluorescein with a K_D of 0.75 nM. The free scFv readily crystallizes by compacting its 18 amino acid-long CDR-H3, partially occluding the binding site and further blocking access by binding to the "bottom" of a neighboring scFv molecule with a cluster of exposed aromatic residues within CDR-H3. Only upon mutating one of the residues involved in this dominant crystal contact, an exposed tryptophan in the middle of CDR-H3, crystals of the complex could be obtained. A series of alanine mutants within the putative antigen binding site, covering a range of binding affinities, were used to relate macroscopic thermodynamic and kinetic binding parameters to single-molecule disruption forces measured by AFM. The effects of the mutations on the binding properties, particularly on the fraction of binding-competent molecules within the population, cannot be fully explained by changes in the strength of local interactions. The significant conformational change of CDR-H3 between the free and the liganded form illustrates the plasticity of the binding site. An accompanying study in this issue by Curcio and colleagues presents the molecular dynamics simulation of the forced unbinding experiments and explores possible effects of the mutations on the unbinding pathway of the hapten.

Keywords: structure/function studies; proteins of the immune system; active site; binding site; epitope mapping; crystallography; protein crystallization; forces and stability; mutagenesis (site-directed and general); atomic force microscopy

The mechanistic understanding of binding and unbinding events of ligands to proteins, in particular defining all of the intermediates in the pathway, will be crucial in the attempts to predict affinities from structures and also in the design of tight-binding inhibitors to a given protein. To simplify such investigations it is of great advantage if at least one of the partners, by necessity the ligand, is rather rigid. Fluorescent ligands such as fluorescein that alter their fluorescence emission upon binding, with an excitation and emission spectrum well separated from the intrinsic fluorescence of the antibody, form ideal model systems for the study of molecular interactions. While in many antibody/antigen pairs the intrinsic Trp fluorescence of the antibody is perturbed upon ligand binding and can also be used to follow interactions with the antigen, the effect is often weak, and the effects of ligand binding cannot always be distin-

Reprint requests to: Andreas Plückthun, Biochemisches Institut der Universität Zürich, Winterthurerstrasse 190, CH-8057 Zürich, Switzerland; e-mail: plueckthun@bioc.unizh.ch; fax: 41-44-635-5712.

Abbreviations: V_H, variable domain of antibody heavy chain; V_L, variable domain of antibody light chain; scFv, single-chain variable fragment of an antibody; FITC, fluorescein isothiocyanate; BSA, bovine serum albumin; wt, wild-type; AFM, atomic force microscopy; CDR, complementarity determining region of an antibody; ORE, Oregon Green 488; PDB, Protein Data Bank.

Article and publication are at http://www.proteinscience.org/cgi/doi/10.1110/ps.051520605.

guished from effects of changes in the protein conformation or even aggregation.

Fluorescent ligands offer the technical advantage that their binding can be followed in real time in solution at the low concentrations required to quantify high affinity interactions. For this reason, antibodies against fluorescein in general and constructs derived from the monoclonal antibody mAb 4-4-20 in particular (Kranz et al. 1982; Herron et al. 1989; Whitlow et al. 1995) have been popular as a model system for the experimental study of fundamental questions of ligand binding to proteins (Herron et al. 1986; Denzin et al. 1991, 1993; Swindlehurst and Voss 1991; Ahlers et al. 1992; Bedzyk et al. 1992; Denzin and Voss 1992; Coelho-Sampaio and Voss 1993; Omelyanenko et al. 1993; Lim et al. 1995; Mummert and Voss 1996) and the computational simulation of these interactions (Lim and Herron 1995; Lim et al. 1995; Paci et al. 2001).

In previous studies (Ros et al. 1998; Schwesinger et al. 2000), the equilibrium affinities and the rate constants for association and dissociation were determined for a range of point mutants derived from three unrelated fluorescein-binding scFvs, and they were correlated to the rupture forces governing the interaction between individual molecules of antibody and hapten measured by atomic force microscopy (AFM).

The first of these antibodies, scFv 4D5-Flu (Jung and Plückthun 1997), was derived from a loop graft of the antigen binding site of the murine monoclonal antibody mAb 4-4-20 (Kranz et al. 1982) on the 4D5 framework (Eigenbrot et al. 1993) to overcome the poor production yield and aggregation-prone behavior of the wild-type 4-4-20 scFv (Essig et al. 1993; Nieba et al. 1997). Since the antigen binding parameters were not altered by the loop graft, this construct relates the results obtained from AFM unbinding experiments (Ros et al. 1998; Schwesinger et al. 2000) to the wealth of data published on the ligand interactions of the antibody 4-4-20. The second scFv, FITC-E2, was selected from a naïve human scFv library by using phage display (Vaughan et al. 1996). A series of mutants with different binding affinities were generated by a partial alanine scan of the putative antigen binding site (Pedrazzi et al. 1997) based on a molecular model. The third scFv, clone 12, was isolated by ribosome display from a murine immune library generated from FITC-BSA immunized mice. This scFv was further improved by in vitro affinity maturation using ribosome display (Hanes and Plückthun 1997), combining error-prone PCR with stringent off-rate selection (Jermutus et al. 2001). The three scFvs utilize different binding interactions with fluorescein, and the point mutants derived from them span a wide range of affinities.

At the time of the analysis, the X-ray structure of the wt 4-4-20 Fab fragment was the only structure of a fluorescein-binding antibody available, (PDB entries 4FAB and 1FLR) (Gibson et al. 1988; Herron et al. 1989, 1994; Whitlow et al. 1995). The structures of two additional members of the 4-4-20 family have been determined more recently, the idiotypically related, medium-affinity Fab 9-40 (PDB entry 1T66) (Terzyan et al. 2004) and the affinity-matured, very high-affinity scFv 4M5.3 (PDB entry 1X9Q) (Midelfort et al. 2004). The four antibodies of the 4-4-20 family all use the same binding mode, the position of the hapten differing by only a fraction of an Ångstrom in the different structures.

In this work, we present the X-ray structures of the free and liganded form of the scFv FITC-E2 (PDB entries 2A9M and 2A9N), which utilizes clearly different binding interactions from the 4-4-20 family of antibodies. The structure of the liganded FITC-E2 scFv allows us to assess on a molecular level the effects of the alanine mutations within the putative antigen interaction site on the binding parameters. In the accompanying study (Curcio et al. 2005), the results of the computational simulation of the forced-unbinding experiments are presented, analyzing the unbinding mechanism of the hapten fluorescein from the wt FITC-E2 scFv and from some of the mutants.

Results

Crystallization of the unliganded FITC-E2 scFv

The unliganded wt scFv readily crystallized in space group $P2_1$ with unit cell dimensions a = 50.96 Å, b = 73.54 Å, c = 70.72 Å, and $\beta = 97.11^{\circ}$. With two molecules in the asymmetric unit (assuming a molecular mass of 27,726 Da) the specific protein volume was Vm = 2.37 $Å^3$/Da, which corresponds to a solvent content of the crystals of 48% (Matthews 1968). However, neither cocrystallization with fluorescein nor with a number of more water-soluble analogs of the hapten yielded any crystals of the liganded scFv, while hapten soaked into preformed crystals of unliganded wt scFv did stain the crystals, but did not localize to a defined position in the structure.

Structure of the unliganded FITC-E2 scFv

The unliganded anti-fluorescein scFv structure was solved by molecular replacement using the Fv fragment of mouse monoclonal antibody D1.3 (PDB entry 1A7N) as starting models. After alternating cycles of refinement with CNS (Brünger et al. 1998) and model adjustment with Turbo-Frodo (Roussel and Cambillau 1991), the final model, at 2.1 Å resolution, has an R-factor of 20.6% and an R_{free} of 26.0% (Table 1). The final model is composed of two scFv molecules in the asymmetric unit and 315 water molecules. The N-terminal short FLAG-tag, V_L residues L1 and L2, the 15 amino acid $(G_4S)_3$ linker, and the C-terminal His_5-tag are not visible

Table 1. *Data collection and refinement statistics for the two structures*

	wt FITC-E2–free	FITC-E2 W129A–complex
Data Collection	100K	RT
Cell dimensions	a = 50.96 Å, b = 73.54 Å, c = 70.72 Å, β = 97.11°	a = 81.38 Å, b = 100.5 Å, c = 61.75 Å
Space group	$P2_1$	$P2_12_12$
Vm / (%) solvent	2.37/48	2.28/46
No. of molecules/a.u.	2	2
Data resolution	2.1	3.0
No. of observations	94,689	62,796
No. of unique	28,656	10,306
Completeness I/σ[I] (overall:last shell)	98.0/97.4	97.4/97.5
R_{sym} % (overall/last shell)	8/22	14/46
Refinement		
No. of reflections	27,558	10,619
Resolution	15.0–2.1	18–3.05
R_{factor} / R_{free}	20.6/26.0	18.2/24.2
No. of atoms	3827	3591
No. of solvent atoms	315	
B-factors (Å^2)		
Main chains	16.6	34.7
Side chains	17.5	34.8
Solvent	21.9	
R.M.S. deviations		
Bonds (Å)	0.011	0.012
Angles (°)	1.4	1.34

in the structure. A fraction of 88.8% of the residues are located in the most favored regions of the Ramachandran plot, 10.7% in the additionally allowed regions, and one residue per scFv (0.5%) in a disallowed region as calculated with PROCHECK (Laskowski et al. 1993). The residue in the disallowed region is Val L67 (L51). (Antibody residue numbering is according to the Honegger nomenclature [Honegger and Plückthun 2001], and the Kabat nomenclature [Kabat et al. 1991] is given in parentheses.) This residue at the tip of the CDR-L2 assumes forbidden torsion angles in the majority of the known V_L structures (150 of 175 nonredundant V_L structures analyzed have torsion angles in the region of $\Phi = 67 \pm 8°$, $\Psi = -46 \pm 12°$, the torsion angles of the remaining 25 structures are widely distributed on the Ramachandran plot).

Upon determining the unliganded structure, it became apparent that a cluster of exposed aromatic residues within CDR-H3, comprising Tyr H128 (H100b), Trp H129 (H100c), His H131 (H100e), Phe H132 (H100f), and Tyr H133 (H100g) was involved in mediating crystal contacts to the "bottom" of a neighboring scFv fragment, thereby providing a tight interaction and also a rigidification of the otherwise rather long and flexible CDR-H3 (Fig. 1). The CDR-H3 "frozen" in this conformation allowed crystal packing, but its altered conformation changes the shape and reduces the size of the hapten binding pocket, while the interaction of CDR-L1, CDR-L2, and CDR-H3 with the bottom of another molecule in the crystal partially obstructs the access to the binding site, as became apparent after having solved the crystal structure of the complex.

To analyze the crystal contacts in detail, the solvent accessible surfaces of each residue of the two molecules in the asymmetric unit were calculated for the isolated molecules and for the two molecules surrounded by their symmetry-related copies, using the program NACCESS (Hubbard and Thornton 1993). The total buried surface between the two molecules in the asymmetric unit (mol 1 and mol 2) was 1387 Å^2, of which 58% were contributed by apolar side-chain atoms, 27% by polar side-chain atoms, and 15% by main-chain atoms. This contact is nearly identical to the crystallographic contact (1125 Å^2), which blocks the hapten binding pocket of the second molecule in the asymmetric unit (mol 2 and mol 1′). Residues within CDR-L1 (L27, L32, L33, and L40 [Kabat L27, L29, L30, and L32]), CDR-L2 (L58–L69 [Kabat L50–L53]), the outer loop of V_L (L82, L84, and H87 [Kabat L66, L68, L69]), and CDR-H3 (H116–H133 [Kabat H100b–H100g]) of one molecule in the asymmetric unit (mol 2 in Fig. 1) pack against a surface formed by the lower loop of V_L (L48–L50 [Kabat L40–L42]), the N-terminal strand a′ of the V_H domain (residues H5–H14 [Kabat H5–H13]), the lower loop of V_H (H46–H48 [Kabat H39–H41]), residues H102 (H88) and H103 (H89), and the C-terminal strand g of V_H (H141–H148 [Kabat H105–H112]) of the other molecule (mol 1), with the four aromatic CDR-H3 residues of mol 2 located in the core of the interface. A symmetry-related copy of molecule 1 (mol 1′ in Fig. 1) is in turn blocked by molecule 2. This interface (between mol 1′ and mol 2) is very similar to the interface between mol 1 and mol 2 in the asymmetric unit. All other crystal contacts are small and loosely packed in comparison to this dominant interface.

Crystallization of the FITC-E2–hapten complex

Based on the structure of the unliganded scFv FITC-E2, we decided to weaken the dominant crystal contact by replacing Trp H129 (H100c) in the center of CDR-H3 with alanine since it had previously been shown that the FITC-E2 Trp H129 Ala mutant not only retained the full ligand binding affinity, but was also produced with better yields than the wt FITC-E2 scFv (Pedrazzi et al. 1997). Because of its somewhat higher water solubility at neutral pH, we used the 5-isomer of the fluorescein analog Oregon Green 488 carboxylic acid (2′, 7′-difluorofluorescein carboxylic acid), rather than fluorescein itself, as a ligand for crystallization (Fig. 2). Oregon Green is isosteric to fluorescein and has the same spectral characteristics. The complex of

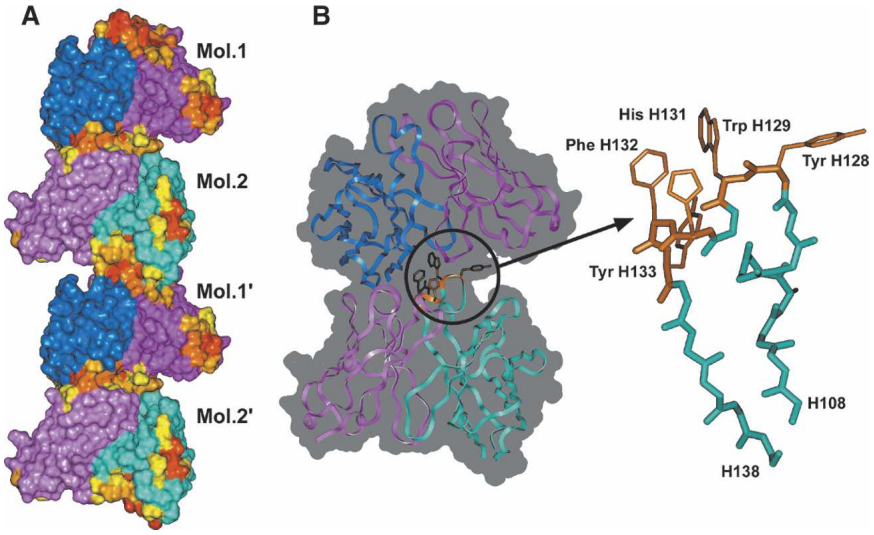

Figure 1. Crystal packing and CDR-H3 conformation in the unliganded FITC-E2 scFv. (*A*) Crystal contacts determine the compact conformation of the long CDR-H3 of FITC-E2, as dominant crystal contacts organize the scFv in the crystal into tightly packed stacks, which pack against each other through smaller crystal contacts. Packing contacts are visualized by color coding the residue according to the fraction of their solvent accessible surface area buried in crystal contacts. Residues that bury > 80% of the solvent accessible surface of the free molecule in crystal contacts are colored red; 60%–80%, orange-red; 40%–60%, orange; 20%–40%, yellow-orange; 1%–20%, yellow. Residues not involved in crystal contacts are colored magenta if located within V_L and blue if located within V_H. The interface between mol 1 and mol 2, the two molecules in the asymmetric unit, is very similar to the interface between mol 2 and mol 1′, an adjacent symmetry related copy of mol 1. (*B*) The aromatic side chains of Tyr H128 (H100b), Trp H129 (H100c), His H131 (H100e), Phe H132 (H100f), and Tyr H133 (H100g) are located at the core of the dominant crystal interface. Packing of these residues against the bottom of a neighboring molecule determines the conformation of CDR-H3, which alters the shape of the hapten binding pocket. Hapten soaked into the crystals of the unliganded antibody did not localize to the binding pocket, and the wt FITC-E2 failed to crystallize in the presence of the hapten. A mutant scFv in which this dominant crystal contact had been disrupted by the replacement of Trp H129 (H100c) by Ala, a replacement shown not to affect antigen affinity, could be crystallized in the presence of antigen and yielded the structure of the complex.

the mutant scFv with the hapten crystallized in the space group $P2_12_12$ (a = 81.38 Å, b = 100.5 Å, c = 61.75 Å). The crystals contain two scFv-FITC-E2–hapten complexes per asymmetric unit, giving a Vm value of 2.28 $Å^3$/Da.

Structure of the FITC-E2 Trp H129 Ala scFv–fluorescein complex

The unliganded FITC-E2 scFv model was used as a starting model for solving the structure of the complex of the Trp H129 (H100c) Ala mutant of the FITC-E2 scFv in complex with the hapten 2′, 7′-difluorofluorescein carboxylate (Oregon Green 488). The same refinement procedure was followed as for the free form, with extensive remodeling of CDR-H3. Once the model was readjusted, the 2′, 7′-difluorofluorescein carboxylate molecule was introduced into the refinement. The asymmetric unit of the 2′, 7′-difluorofluorescein-complexed scFv contains two scFv molecules and two hapten molecules. The final R-factor is 18.2% (R-free = 24.2%) at 3.0 Å resolution (Table 1) and 82.8% of the residues are located in the most favorable area of the Ramachandran map, 16.2% in additionally allowed regions as calculated with PROCHECK (Laskowski et al. 1993). Again, Val L67 (L51) assumes torsion angles in a disallowed region. The 2′, 7′-difluorofluorescein molecules are well defined in density, despite the rather limited diffraction of the crystals (Fig. 3).

In the liganded FITC-E2 structure, the CDRs are only involved in weak crystal contacts. The N- and the C-terminal strands of the V_H domain, which in the unliganded structure packed against the antigen binding site of a neighboring molecule, now interact symmetrically with the corresponding V_H regions of the second molecule in the asymmetric unit. With a total buried surface of 1124 $Å^2$, this strong contact is the dominant crystal contact in the liganded structure. Other, weaker crystal contacts involve part of CDR-H2, the outer loop of V_H and the tip of CDR-H3, as well as the bottom and the outer loop of the V_L domain.

Comparison of the free and the liganded structure

Superposition of the two monomers of the anti-fluorescein scFv in the free form yields an RMSD of 0.6 Å for all

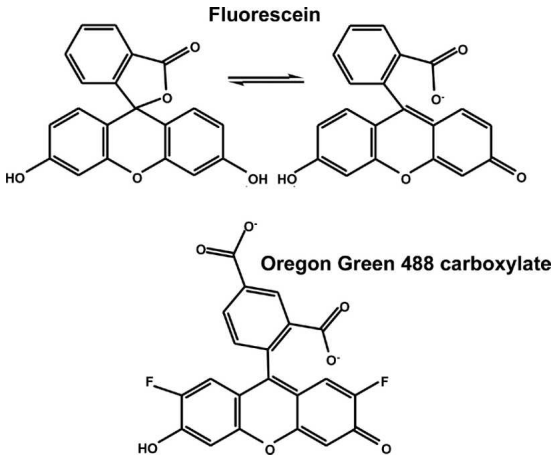

Figure 2. Comparison of the haptens fluorescein and Oregon Green 488 carboxylate. For fluorescence titrations, free fluorescein was used. In the crystal, the open ring form is present, and the carboxylate group interacts with an arginine in the binding pocket (Fig. 5). For determining the crystal structure, the carboxylated and difluorinated analog Oregon Green 488 carboxylate (ORE) was used.

Cα positions visible in the V_L and V_H chains (Table 2). These deviations have a larger amplitude within loops. In the complexed form of the anti-fluorescein scFv, the RMSD between the two monomers in the asymmetric unit is lower (0.34 Å) due to the use of restrained refinement, itself motivated by the lower resolution of the data sets. However, in both cases, the deviations remain within the usual range of values. Much larger RMSD values are observed between the free and complexed anti-fluorescein scFvs after superposition (Table 2; Fig. 4). The RMSD between the two molecules 1 and the two molecules 2 are 1.58 Å and 1.75 Å, taking into account all C_α atoms in the comparison. If CDR-H3 is omitted from the comparison, the RMSD is reduced to 0.83 and 0.96 Å, as the conformation of the 18 amino acid long CDR-H3 differs considerably between the free and the liganded form (Table 2).

When the V_L and V_H domains of the free and liganded molecules 1 are compared separately, a RMSD of 0.42 Å and 0.43 Å is observed between the V_L domains of the Cα atoms of the free and the complexed structure, while a value of 0.63 Å and 0.54 Å is measured for V_H, excluding CDR-H3 (Table 2). The smaller values obtained for the single domain superposition, compared with the scFv superposition, indicate that a rigid body motion of V_L versus V_H occurs upon complexation (Fig. 4). This movement can be described by a 3° rotation of the V_H domain around a horizontal axis in the plane of Figure 4. The motion would narrow the hapten binding pocket, except that at the same time, residues H130–H134 (H100d–H100h) of CDR-H3 move up and out of the hapten binding pocket in the liganded structure. Optimal alignment of the aromatic CDR-H3 side chains involved in the dominant crystal contact of the unliganded structure to a hydrophobic patch on the neighboring molecule necessitates the compact conformation of CDR-H3 (Fig. 1). The relative orientation of the domains in the complex structure is not compatible with this compact CDR-H3 conformation, as this combination would lead to clashes between the side chain of Tyr H135 (100i) with that of Leu L54 (L46), the side chain of Tyr H133 (H100g) with the side chain of Asp L58 (L50), and of the main-chain CO of Phe H132 (H100f) with the Cβ of Tyr L40 (L32). Since residues Tyr H128 (H100b), Trp H129 (H100c), His H131 (H100e), Phe H132 (H100f), and Tyr H133 (H100g) in CDR-H3 are strongly involved in crystal contacts in the unliganded form of FITC-E2, and since the mutation of Trp H129 (H100c) to Ala was necessary to break this dominant contact and to allow the growth of

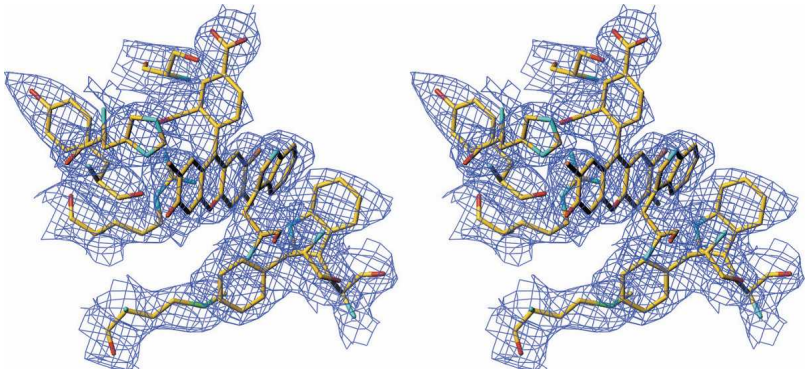

Figure 3. Electron density around the hapten (stereo view). Despite the relatively low resolution of the structure of the FITC-E2–hapten complex, the electron density around the hapten is well defined. The hapten is shown surrounded by binding pocket residues Met H136, Phe L137, Trp H54, Trp L109, Ser H59, His H131, Tyr H133, and Arg H109.

Table 2. *Root mean square deviation (Å) between the FITC-E2 structures*

		V_L	V_H	$V_H^{-CDR-H3}$	Fv	$Fv^{-CDR-H3}$
No. of Cα atoms		107	126	108	233	215
Free mol 1	Free mol 2	0.49	0.61	0.55	0.60	0.55
Free mol 1	Complex mol 1	0.42	1.89	0.63	1.58	0.83
Free mol 2	Complex mol 2	0.43	1.94	0.54	1.75	0.96
Complex mol 1	Complex mol 2	0.30	0.28	0.25	0.34	0.34

Root mean square deviation in Å between the C_α positions of the two molecules in the asymmetric unit of the free (free mol 1 and free mol 2) and the complexed scF_V FITC-E2 (complex mol 1 and complex mol 2) and between free and complexed structures, for the V_L domains, the V_H domains and the V_H domains excluding CDR-H3 ($V_H^{-CDR-H3}$), and the Fv fragments and finally the Fv fragments excluding CDR-H3 ($Fv^{-CDR-H3}$).

crystals containing the hapten complex, the crystal environment most likely causes this conformational change of CDR-H3, and, mediated by the change in CDR-H3 conformation, indirectly affects the domain orientation. The V_L domain does not undergo any conformational changes in this process (Fig. 4). In solution, the long CDR-H3 loop might be quite flexible and not assume a unique conformation. Hapten binding might affect the relative domain orientation as well, as the hapten interacts with both the V_L and the V_H domain.

Antibody–hapten interactions

The 2′, 7′-difluorofluorescein carboxylate molecule is deeply buried between the V_H and the V_L domains (Fig. 4). An area of 762 $Å^2$ (molecule 1) to 783 $Å^2$ (molecule 2) of solvent accessible surface is buried in the interaction between hapten and antibody; 82% of the total accessible surface of the free hapten is inaccessible in the complex. The hapten interacts mainly with three loops of the scFv, i.e., L3, H2, and H3 (Fig. 4; Table 3). The fused rings are located at the bottom of the cavity, while the polar end, the phenyl ring bearing the two carboxylates, points toward the bulk solvent. This can be rationalized, since originally the FITC-E2 scFv was selected for binding to FITC coupled to BSA, which corresponds to a linkage via the para-carboxylate group. For molecules 1 and 2, 473–492 $Å^2$ of the surface of the hapten are buried upon complexation and it covers 289–291 $Å^2$ of the surface of the scFv molecules, mainly at the level of CDR-L3, CDR-H1, and CDR-H3 (Table 3). The binding pocket accommodating fluorescein is predominantly lined with aromatic and polar residues (Fig. 5). The side chain of Trp L109 (L91) is almost parallel to the xanthene group of fluorescein, while at the bottom of the cavity, Phe L137 (L96) interacts with the xanthene ring oxygen. Polar interactions with the hapten play an important role in binding; Arg H109 (H95) establishes an ionic bond with the lateral carboxylate, Trp H54 (H47) hydrogen-bonds to O1; Ser H42 (H35) and H59 (H52) hydrogen-bond to O1 and COO^-, respectively; His H131 (H100e) interacts with F2 of the 2′, 7′-difluorofluorescein carboxylate (Fig. 5A). The binding pocket is large enough that the replacement of the hydrogen atoms in the 2′ and 7′ position of the fused ring system of the original hapten by bulkier halogen atoms does not interfere with binding.

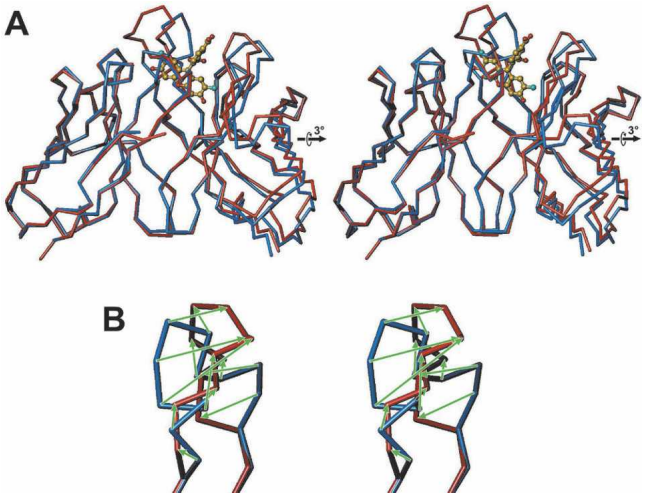

Figure 4. Alignment of free and liganded structure and detailed comparison of CDR-H3 conformation. (*A*) Least squares superposition of V_L in the unliganded FITC-E2 scFv (blue) and the FITC-E2–hapten complex (red), indicating the difference in the relative orientation of V_L and V_H in the two structures. The axis of a 3° rotation relating the V_H orientations in the free and the liganded scFv, located in the plain of the figure, is indicated by a small arrow. (*B*) CDR-H3 conformation in the unliganded scFv (blue) and the liganded scFv (red). Equivalent atoms are related by green arrows.

Comparison of the fluorescein complexes FITC-E2 Trp H129 Ala and FAB-4-4-20

The structures of the Oregon Green 488–FITC-E2 Trp H129 Ala complex and of the fluorescein–FAB-4-4-20 complex (4FAB) were superimposed by a least squares fit of a total of 150 residues (cutoff 2.0 Å), giving an RMSD of 1.16 Å between the two structures (Fig. 6).

Table 3. *Details of antibody–hapten interactions (reduction of solvent accessible area)*

	FITC-E2 interacting residues	FITC-E2 Mol 1 (Å^2)	FITC-E2 Mol 2 (Å^2)	4-4-20 Family[a]
CDR-L1	Asn L39, Tyr L40	12	8	89 ± 8
CDR-L2	—	0	0	3 ± 4
CDR-L3	Trp L109, Phe L137	74	77	19 ± 2
CDR-H1	Ser H42	0.5	1.4	61 ± 4
CDR-H2	Trp H54, Gly H57, Leu H58, Ser H59, Leu H67, His H69	85	83	38 ± 10
CDR-H3	Arg H109, Gly H130, His H131, Tyr H133, Ser H234, Met H136	118	122	70 ± 5
Total Fv[b]		289	291	280 ± 11
Hapten free[c]	ORE (FITC-E2), FLU (4-4-20)	658	670	489 ± 5
Hapten bound[d]		185	178	62 ± 13
Difference free-bound[e]		473	492	427 ± 14

Solvent accessible surfaces were calculated according to Lee and Richards (1971) using the program NACCESS (Hubbard and Thornton 1993).
[a] Average of four structures: 4FAB, 1FLR, 1T66, 1X9Q.
[b] Total Fv surface area buried by hapten.
[c] Total surface area of free hapten.
[d] Accessible surface area of hapten when complexed by antibody.
[e] Hapten surface buried by antibody.

Two striking features can be noticed at once: (1) the CDR-H3 loop of FITC-E2 Trp H129 Ala is much longer than that of FAB-4-4-20 (18 amino acids vs. 7 amino acids, double arrow in Fig. 6) and occupies the position of fluorescein in the 4-4-20 complex, and (2) the hapten fluorescein in FITC-E2 is rotated and shifted relative to its orientation and position in 4-4-20. The main movements are two 90° rotations around one axis horizontal in the plane and perpendicular to the plane and a shift to the left of the figure.

The long CDR-L1 of 4-4-20 and a Trp in position H40 (H33) of CDR-H2 contribute significantly to hapten binding in the 4-4-20 family of antibodies (4FAB, 1FLR, 1T66, and 1X9Q). CDR-L1 and -H1 together contribute around 50% of the antibody surface buried by the hapten. In FITC-E2, these two CDRs contribute only 3%–4% of the interaction surface, while the longer λ-CDR-L3, CDR-H2, and CDR-H3 make a larger contribution than they do in the 4-4-20 family. Despite these differences, the antibody surface areas buried upon complexation of the immunoglobulin fragments FITC-E2 Trp H129 Ala and the four members of the 4-4-20 family are comparable, 290 ± 2 and 280 ± 11 Å^2, respectively (see Table 3 for details).

Effects of Ala-scan mutations

The original point mutants were designed based on a homology model of FITC-E2 (Pedrazzi et al. 1997). The point mutations were introduced individually into the wt FITC-E2 scFv and their effects on the equilibrium binding characteristics and binding kinetics were assessed by fluorescence titration, and their effects on the force required to rupture the interaction between a single hapten molecule and a scFv were assessed by atomic force microscopy as described previously (Pedrazzi et al. 1997; Ros et al. 1998; Schwesinger et al. 2000). Although the binding site area was properly chosen based on a homology model of the scFv, the exact placement of the hapten in the binding site was not known, and the complications introduced by the H3 loop conformational change were not predictable.

The affinities of the mutants to fluorescein are summarized in Table 4. Residues Asn L39 (L31), Asp L111 (L93), Arg H61 (H53), Leu H67 (H56), and Trp H129 (H100c) are not in a position to interact with fluorescein (Fig. 7), and consequently, the corresponding Ala mutants have the same affinities as the wt scFv. Arg H109 (H95) interacts with the ortho-carboxylate of the hapten (Fig. 5); its mutation results in a total loss of fluorescein binding (Table 4). His H131 (H100e) interacts with a fluorine atom of 2′, 7′-difluorofluorescein carboxylate, but may not interact with the corresponding hydrogen of fluorescein; its mutation results in only a twofold increase of the K_D of fluorescein. Phe H132 (H100f) is turned outside the combining site in the liganded structure; the observed fourfold increase of the K_D upon mutation to Ala can only be explained by invoking an indirect effect on the conformation of a neighboring side chain or on the H3 loop ability to change conformation. Tyr H133 (H100g) Cβ is in weak contact with the ortho-carboxylate; it is unclear whether this explains that

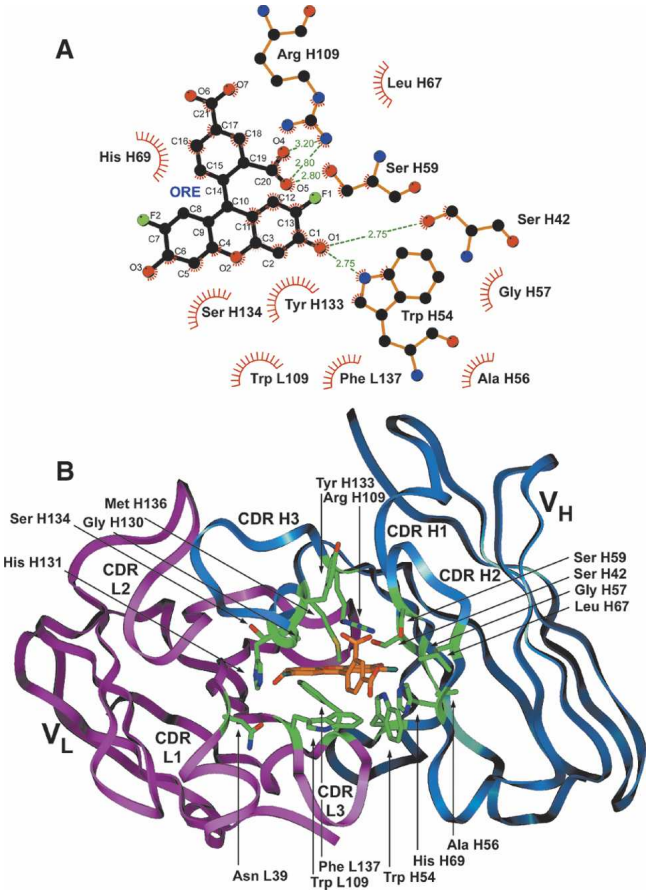

Figure 5. Details of antibody–hapten interactions. (*A*) Ligplot (Wallace et al. 1995) representation of the interactions between the hapten and the antibody. (*B*) Location of the residues lining the hapten binding pocket of the antibody.

mutation to Ala leads to a threefold increase of the K_D, and indirect effects may play a role as well. His H69 (H58) interacts with the para-carboxylate of the hapten Oregon Green 488 in the liganded structure, with a distance between the Nδ of the imidazole ring and one of the oxygens of the carboxylate of 3.4 Å (Figs. 5B, 6). However, this interaction cannot explain the affinity difference for fluorescein, since this carboxylate group is not present in the free fluorescein used for fluorescence titration, and it is replaced by a thiourea group produced when fluorescein isothiocyanate was coupled through a linker to the cantilever tip for AFM measurements (Ros et al. 1998). Thus, from the static picture offered by the X-ray structure, it is unclear why the His H69 (H58) Ala mutation provokes a 10-fold decrease in affinity (Table 4). Interestingly, this mutation increases the off-rate by a factor of about 10^2 and the on-rate by a factor of about 10 (Schwesinger et al. 2000), suggesting that a barrier is removed. The unbinding simulations of Curcio et al. (2005) offer a possible explanation, as the interaction of His H69(H58) with the hapten seems to be related to the existence of a metastable intermediate on the major unbinding pathway, which is not observed in the Ala mutant.

For some of the mutants, the binding curves could only be fitted if not only the K_D, but also the number of binding sites was treated as a variable to be fitted (data shown in Pedrazzi et al. 1997). Thus, in these mutants the concentration of binding-competent scFv was significantly lower than was expected based on the protein concentration. For mutations Ser H59 (H52) Ala the fitted concentration of active molecules amounted to only 1% of the protein concentration, for Trp H54 (H47) Ala to 3%, for Trp L109 (L91) Ala to 7%, and for His H69 (H58) Ala to 29% of the expected concentration. This reduction in the number of binding sites could not be linked to the presence of multimers, aggregates, or partially degraded species. It was not only observed with the free scFv, but was already seen in the phages displaying the corresponding mutants.

Discussion

Antibodies binding to fluorescein have become an important model system to study the details of ligand binding since the system is greatly simplified by the rigidity of the ligand and the fact that ligand binding can be conveniently followed in solution. Since the antibodies are selected from a carrier-bound form in which fluorescein is linked to a protein support, such as in the FITC-BSA conjugate, via a linker to an isothiocyanate group on the phenyl group para to the xanthene moiety, the latter will by necessity be buried in the protein. In the present structure of FITC-E2,

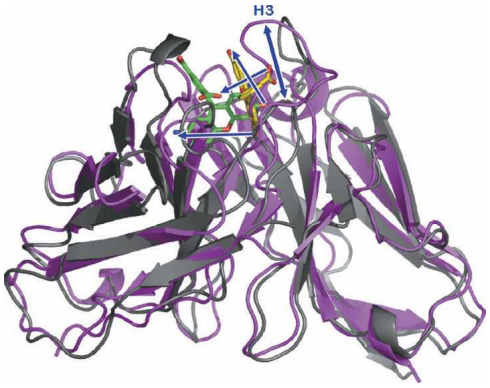

Figure 6. Ribbon plots of the fluorescein complexes of FITC-E2 Trp H129 Ala (magenta) and FAB-4-4-20 (gray). The hapten carbon atoms in the two structures are colored green (FITC-E2) and yellow (4-4-20). The difference between the two H3 loops is highlighted by a blue double arrow, and the equivalent atomic positions between the two haptens are related by blue arrows (figure made with PyMol [http://www.pymol.org]).

Table 4. *Effects of alanine mutations on the fluorescein-binding characteristics in the FITC-E2 scFv*

Mutations	K_D tit. [nM][a]	Activity [%][b]	k_{off} [s^{-1}][c]	k_{on} [10^6 $M^{-1}s^{-1}$][c]	K_D tit. [nM][c]	K_D calc. [nM][c]
wt	0.75	86	0.0044	1.8	1.1	2.4
Asn L39 Ala	0.74	87				
Trp L109 Ala	0.71	7				
Asp L111 Ala	0.93	80				
Trp H54 Ala	0.74	3				
Ser H59 Ala	0.97	1				
Arg H61 Ala	0.63	83				
Leu H67 Ala	0.74	84	0.0125	2.5	1.8	5
Thr H68 Ala	0.83	70				
His H69 Ala	8.9	29	0.47	11.9	15	39
Asp H72 Ala	0.73	68				
Arg H109 Ala	n.d	0				
Trp H129 Ala	0.71	89				
His H131 Ala	1.6	91	0.0052	1	2.7	5.2
Phe H132 Ala	2.9	70	0.0062	0.3	9.6	20
Tyr H133 Ala	3.1	67	0.019	1	7.9	19

[a] K_D values determined by fluorescence titration (Pedrazzi et al. 1997).
[b] The relative activity of the scFv preparation indicates the fraction of active molecules, derived from the discrepancy between the theoretical number of binding sites calculated from the protein concentration and the concentration of binding sites determined by fluorescence titration (Pedrazzi et al. 1997).
[c] Off-Rates, on-rates, K_D calculated from k_{on}/k_{off} and equilibrium K_D from titration are from Schwesinger et al. (2000).
(n.d.) No binding detectable.

the pseudo twofold axis of the scFv almost bisects the short axis of the xanthene moiety. In contrast, in 4-4-20 (Gibson et al. 1988; Herron et al. 1989, 1994; Whitlow et al. 1995), the xanthene moiety is buried, but at an angle to the pseudo twofold axis. In both cases, as in the case of a lipocalin selected from a library (Korndorfer et al. 2003) (PDB ID 1N0S), the xanthene is almost fully buried and adjacent to aromatic residues.

The scFv FITC-E2 was one of the three anti-fluorescein scFv fragments with which the relationship between kinetics and thermodynamics of binding was established (Ros et al. 1998; Schwesinger et al. 2000). It was also used as a model system to establish the "selectively-infective phage" (SIP) selection technology (Krebber et al. 1995, 1997) for non-peptidic antigens. For both approaches, a set of mutants was required that differ in affinity. Thus, a panel of 16 closely related scFv was produced by an incomplete Ala-scan of the putative antigen binding site of the FITC-E2 scFv, based on a homology model of the scFv (Table 4) (Pedrazzi et al. 1997). However, apart from one mutation that almost completely abolished binding (Arg H109 (H95) Ala), the range of affinities spanned by the different mutants was surprisingly narrow, with only one order of magnitude between the lowest and the highest affinity measured. Interestingly, a number of mutations dramatically decreased the fraction of active molecules, yet without noticeably altering the level of soluble expression.

In Figure 7, the experimentally determined structure of the hapten complex is depicted. Residues altered in the Ala scan have been color coded according to the effects of the mutations on the functional characteristics of the mutants (Table 4). Residues that drastically decreased the fraction of active molecules are shown in red. Trp L109 (H95) Ala significantly altered the binding curve, indicating weaker binding, as can be expected from the structure, but a satisfactory fit could only be obtained if the fraction of active molecules was reduced to only 7% of the number of binding sites expected based on protein concentration (Pedrazzi et al. 1997). It should be noted that the K_D value derived from fluorescence titration is not very accurate in this case. While we cannot rule out a more complicated model with several states of lower affinity, this result does suggest a conformational change in the binding site caused by this mutation, with a slow equilibrium between a binding-incompetent, inactive form of the scFv and a binding-competent, active one. While for some other scFvs aggregation and precipitation of misfolded molecules has been observed, the Ala mutations did not lead to noticeably unstable, insoluble, or aggregation-prone proteins (Pedrazzi et al. 1997). While the comparison of the free and the liganded structure shows two different states within the conformational repertoire of the FITC-E2, the binding-incompetent conformation in the hapten-free structure is not necessarily the same as the binding-incompetent state in solution, since the conformation of the hapten-free structure is governed by intermolecular interactions in the crystal, and the mutations that lead to a decreased fraction of active molecules in solution are unlikely to stabilize this particular conformation.

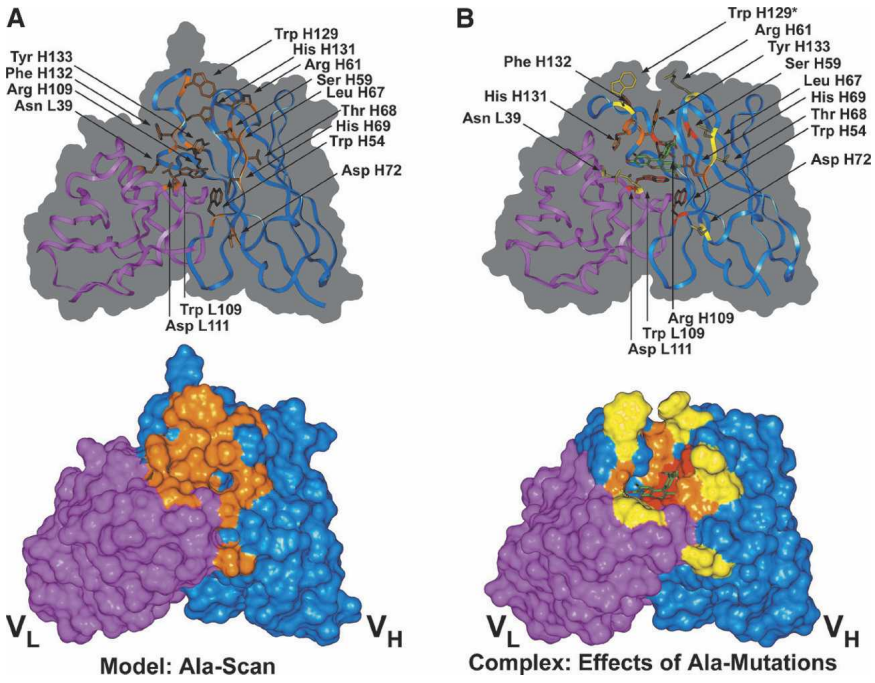

Figure 7. Results of the alanine scan of the antigen binding site of FITC-E2. (*A*) Location of the mutated residues (orange) in the homology model used to design the Ala scan. (*B*) Ala-mutations are color coded according to their effects on antigen binding in the wireframe (*top*) and solvent accessible surface (*bottom*) representation of the experimental structure of the liganded FITC-E2 scFv. H129, mutated to Ala to obtain crystals of the hapten complex, has been replaced by the Trp present in the wt FITC-E2 in the molecule shown. Residues Trp L109 (L91), Trp H54 (H47), Ser H59 (H52), and Arg H109 (H95), whose replacement by Ala predominantly altered the fraction of active scFv (fitted number of hapten binding sites divided by the number of binding sites expected according to the protein concentration) without disturbing the binding affinity, are colored red. Residues His H69 (H58), His H131 (H100e), Phe H132 (H100f), and Tyr H133 (H100g), whose replacement by Ala reduced the hapten binding affinity, are shown in orange. Residues Asn L39 (L31), Asp L111 (L93), Arg H61 (H53), Leu H67 (H56), Thr H68 (H57), Asp H72 (H61), and Trp H129 (H100c), whose replacement by Ala had no major effect on hapten binding are shown in yellow. Trp H129 Ala proved to be superior to the wt in selective interactive phage selection, due to its better folding efficiency. The mutation also improved the production yield in periplasmic production in *E. coli*.

Arg H109 (H95) Ala completely abolished ligand binding. While the guanidino group of the arginine residue interacts with the ortho carboxylate of the ligand and thus contributes directly to the binding of the hapten, a mutation to alanine may also allow CDR-H3 to take on a different conformation, thereby disrupting even more interactions. Mutation of Ser H59 (H52) to Ala, affecting a residue located in the immediate neighborhood of Arg H109, which hydrogen bonds both to the arginine guanidino group and the ortho carboxylate of the hapten (Fig. 5), severely interferes with antigen binding. As in the case of the Trp L109 (H95) Ala mutation, the effect of the mutation on the antigen binding curve cannot be fitted by assuming only a reduction of the binding affinity, but the effect rather corresponds to a reduction in the concentration of active molecules to 1% of the expected value.

Alanine mutations of the highly conserved Trp H54 (H47) (94% Trp in murine, 96% Trp in human V_H) and of Trp L109 (L91) (97% Trp in murine Vλ, 43% Trp and 38% Tyr in human Vλ) to Ala represent mutations in residues which serve a dual role, not only contributing to antigen binding, but also contributing significantly to the interface between the V_L and the V_H domain. Such mutations can be expected to have a strong effect on the domain interactions, affecting both the stability of the interaction and the relative orientation of the domains.

Mutants in which one of the residues indicated in orange had been changed to Ala were still able to bind the antigen, but with decreased affinity. However, the effects were surprisingly weak. Replacement of His H69 (H58) in CDR-H2 by Ala had the strongest effect, reducing the affinity by a factor of 12 while reducing the fraction of active molecules to a third. Replacing any of the adjacent residues His H131 (H100e), Phe H132 (H100f), or Tyr H133 (H100g) by Ala reduced the affin-

ity two- to fourfold; all other residues tested (indicated in yellow) had no significant effect on antigen binding.

It required mutagenesis to obtain the structure of the complexed scFv, as it was not possible to obtain crystals of the wt scFv in the presence of the hapten. A closer look at the packing interactions within the crystals showed that several exposed aromatic residues within the rather long CDR-H3 (18 residues) pointed away from the scFv, and then packed together and into a hydrophobic depression in the bottom of the neighboring scFv (Fig. 1). Residues Tyr H128 (H100b), Trp H129 (H100c), His H131 (H100e), Phe H132 (H100f), and Tyr H133 (H100g) were strongly involved in crystal contacts, thus fixing the conformation of the loop. Tyr H128 (H100b) interacted with Pro L48 (L40), Trp H129 (H100c) with Pro H48 (H41), and the group consisting of Gly L49 (L41), Val H103 (H89), Phe H132 (H100f), and Tyr H133 (H100g) with Leu H144 (H108) of a second scFv in the crystal. The two flanks of the CDR-H3 in the unliganded structure formed short helical segments responsible for the compact and rigid structure of the CDR. The particular CDR-H3 conformation observed in the unliganded structure was obviously governed by the intermolecular interactions of the major crystal contacts, and this conformation apparently is not compatible with antigen binding. The Ala-scan of the binding site had shown that one of the residues critically involved in these CDR-H3 crystal contacts, Trp H129 (H100c), was not only not needed for antigen binding, but its replacement by Ala led to a construct that was produced at higher yields than the wt in the periplasm of *Escherichia coli*. The Trp H129 (H100c) Ala mutant also outperformed the wt and all other Ala mutants tested in SIP selection (Pedrazzi et al. 1997), proving the superior overall performance of that mutant. This mutant then yielded crystals of the complex of the FITC-E2 scFv with 2′, 7′-difluorofluorescein carboxylate.

This structure of the complex has been instrumental in performing a molecular dynamics simulation study of the forced unbinding process (Curcio et al. 2005). Given the considerable flexibility of the antigen recognition site observed here and in many other antibodies (e.g., Schulze-Gahmen et al. 1993; de la Cruz et al. 1994; James et al. 2003), a highly flexible ligand such as a peptide or a large antigen such as a folded protein would increase the complexity of the system considerably and would render the computational simulation and analysis of the interaction much more difficult. Therefore, the use of rigid fluorescent haptens in conjunction with very tight binding proteins may help our understanding of the mechanism of ligand binding and unbinding. The conformational adaptability of CDR-H3 remains a challenge in modeling and in a quantitative interpretation of mutant data. Simulation of binding and unbinding processes may shed light onto these important phenomena.

Materials and methods

Expression and purification of wt and mutant scFv fragments

The gene for the scFv fragment of FITC-E2 was provided by Dr. Kevin Pritchard (Cambridge Antibody Technology). Site-directed mutagenesis was carried out with SIP fCKC-E2, encoding the wt scFv FITC-E2 (Krebber et al. 1997), by the method of Kunkel et al. (1991) and confirmed by sequencing. The mutated scFv gene was recloned as SfiI–SfiI cassette into the expression vector pAK400 (Krebber et al. 1997). The scFv fragments were produced by periplasmic expression in *Escherichia coli* SB536 (Bass et al. 1996) and purified over a Ni^{2+}-NTA column (Qiagen), followed by ion exchange chromatography on a Sepharose-SP column (Pharmacia) in 20 mM MES, 50 mM NaCl (pH 6.0), and subsequent elution with a NaCl gradient as published (Pedrazzi et al. 1997; Schwesinger et al. 2000).

Homology modeling and design of the Ala-scan

The alanine scan of the hapten binding pocket of FITC-E2 was based on a homology model of the FITC-E2 Fv fragment (Pedrazzi et al. 1997). The model was built using the HOMOLOGY module of the INSIGHTII software package (Accelrys). The λ V_L domain was modeled based on the structures of the V_L domain of Fab fragment KOL (PDB entries 2FB4 and 2IG2, 71% sequence identity, 80% similarity, 1.9 Å, and 3.0 Å resolution). The model of the V_H domain was based on the structure of PDB entry 2FBJ (1.95 Å res., 64% ident., 73% sim.). CDR-H3 was modeled in an open conformation typical for hapten binding antibodies, which usually accommodate their ligands in a binding pocket located underneath CDR-H3. Since no appropriate modeling template for the conformation of the 18 amino acid CDR-H3 loop was available, and since loops of that size can be expected to be very flexible, six amino acids at the base on either side of the CDR-H3 were modeled using the CDR-H3 of PDB entry 1DFB as a template, while the six residues at the tip of the CDR were modeled using a conformational search, followed by molecular dynamics annealing.

Crystallization

Crystals of the unliganded anti-fluorescein scFv FITC-E2 were obtained using the hanging-drop method at 20 °C. Drops of 2 μL (protein concentration 2 mg/mL) of the unliganded scFv FITC-E2 were mixed with 2 μL of the well solution (1.6 M ammonium sulfate, 150 mM sodium citrate at pH 5.5).

The complex between the hapten Oregon Green 488 carboxylic acid 5-isomer (2′,7′-difluorofluorescein carboxylic acid, Molecular Probes, CAS 198139-50-3) and the mutant scFv FITC-E2 Trp H129 Ala was prepared by simply mixing both components in a 1/5 molar ratio. Drops of 3 μL of the complex (protein concentration 3 mg/mL) were mixed with 1 μL of a solution containing 29%–30% (w/v) PEG 8000, 0.2 M ammonium sulfate, 10 mM sodium acetate (pH 4.1).

Data collection and processing

Data of the wt free scFv FITC-E2 were collected at 100 K at a synchrotron-radiation source, beamline ID14-EH4, at the Euro-

pean Synchrotron Radiation Facility. Crystals were frozen using 23% glycerol and diffracted to 2.1 Å. Data of scFv FITC-E2 Trp H129 Ala–hapten complex were collected on a MAR-Research Imaging Plate (MAR) placed on a Rigaku RU200 rotating anode using the CuKα wavelength at room temperature. Data integration and reduction from both free and complex scFv FITC-E2 datasets was performed using DENZO (Otwinovski 1993) and SCALA (Bailey 1994) (Collaborative Computational Project, Number 4, 1994, CCP4). The statistics of the data sets are shown in Table 1.

Structure determination and refinement

Both structures were solved by molecular replacement (Rossman and Blow 1962) using the program AMoRe (Navaza 1990, 1994; Navaza and Saludjian 1997). Rotation and translation searches were performed using the structure of the Fv fragment of mouse monoclonal antibody D1.3 (PDB entry 1A7N) for the unliganded wt scFv FITC-E2 and the structure of the free scFv FITC-E2 for the complex of the scFv FITC-E2 Trp H129 Ala with the hapten. The rotation and translation functions were calculated using the data in the resolution range 10.0 and 3.3 Å for both proteins. The molecular replacement solution for the unliganded scFv FITC-E2, which includes two protein molecules per asymmetric unit, gave a correlation coefficient of 38% and an R-factor of 47%. For the complex scFv FITC-E2 Trp H129 Ala with the hapten, the correlation coefficient and the R-factor were 45% and 47%, respectively. Standard CNS and REFMAC protocols were then used successively. The unliganded structure was refined using then REFMAC restrained refinement protocol without NCS restraints. In the complex structure, due to its low resolution, NCS restrained were introduced in the REFMAC protocol, medium for the main chain and loose for the side chains (REFMAC defined options). A few final cycles were performed without any NCS restraints. After each refinement cycle, a new map was calculated and the model rebuilt using the molecular modeling program Turbo-Frodo (Roussel and Cambillau 1991). Final refinement data are summarized in Table 1. The two structures have been deposited in the RCSB Protein Data Bank (http://www.rcsb.org/pdb) and can be accessed as PDB entries 2A9M (unliganded FITC-E2) and 2A9N (FITC-E2–ORE complex)

Acknowledgments

We are grateful to Falk Schwesinger for help in the protein purification and helpful discussions. This work was supported by the Schweizerischer Nationalfonds grant 3100-065344/2.

References

Ahlers, M., Grainger, D.W., Herron, J.N., Lim, K., Ringsdorf, H., and Salesse, C. 1992. Quenching of fluorescein-conjugated lipids by antibodies. Quantitative recognition and binding of lipid-bound haptens in biomembrane models, formation of two-dimensional protein domains and molecular dynamics simulations. *Biophys. J.* **63:** 823–838.

Bailey, S. 1994. The CCP4 suite—Programs for protein crystallography. *Acta Crystal. Sect. D. Biol. Crystal.* **50:** 760–763.

Bass, S., Gu, Q.M., and Christen, A. 1996. Multicopy suppressors of prc mutant *Escherichia coli* include two HtrA (DegP) protease homologs (HhoAB), DksA, and a truncated RlpA. *J. Bacteriol.* **178:** 1154–1161.

Bedzyk, W.D., Swindlehurst, C.A., and Voss Jr., E.W. 1992. Relative binding properties of fluorescein and 9-hydroxyphenylfluoron (HPF) with murine monoclonal anti-fluorescein antibodies. *Biochim. Biophys. Acta* **1119:** 27–34.

Brünger, A.T., Adams, P.D., Clore, G.M., DeLano, W.L., Gros, P., Grosse-Kunstleve, R.W., Jiang, J.S., Kuszewski, J., Nilges, M., Pannu, N.S., et al. 1998. Crystallography & NMR system: A new software suite for macromolecular structure determination. *Acta Crystal. Sect. D. Biol. Crystal.* **54:** 905–921.

Coelho-Sampaio, T. and Voss Jr., E.W. 1993. Pressure-induced dissociation of fluorescein from the anti-fluorescein single-chain antibody 4-4-20. *Biochemistry* **32:** 10929–10935.

Curcio, R., Caflisch, A., and Paci, E. 2005. Change of the unbinding mechanism upon a mutation: A molecular dynamics study of an antibody–hapten complex, *Protein Sci.* **14:** (this issue).

de la Cruz, X., Mark, A.E., Tormo, J., Fita, I., and van Gunsteren, W.F. 1994. Investigation of shape variations in the antibody binding site by molecular dynamics computer simulation. *J. Mol. Biol.* **236:** 1186–1195.

Denzin, L.K. and Voss Jr., E.W. 1992. Construction, characterization, and mutagenesis of an anti-fluorescein single chain antibody idiotype family. *J. Biol. Chem.* **267:** 8925–8931.

Denzin, L.K., Whitlow, M., and Voss Jr., E.W. 1991. Single-chain site-specific mutations of fluorescein-amino acid contact residues in high affinity monoclonal antibody 4-4-20. *J. Biol. Chem.* **266:** 14095–14103.

Denzin, L.K., Gulliver, G.A., and Voss Jr., E.W. 1993. Mutational analysis of active site contact residues in anti-fluorescein monoclonal antibody 4-4-20. *Mol. Immunol.* **30:** 1331–1345.

Eigenbrot, C., Randal, M., Presta, L., Carter, P., and Kossiakoff, A.A. 1993. X-ray structures of the antigen-binding domains from three variants of humanized anti-p185HER2 antibody 4D5 and comparison with molecular modeling. *J. Mol. Biol.* **229:** 969–995.

Essig, N.Z., Wood, J.F., Howard, A.J., Raag, R., and Whitlow, M. 1993. Crystallization of single-chain Fv proteins. *J. Mol. Biol.* **234:** 897–901.

Gibson, A.L., Herron, J.N., He, X.M., Patrick, V.A., Mason, M.L., Lin, J.N., Kranz, D.M., Voss Jr., E.W., and Edmundson, A.B. 1988. Differences in crystal properties and ligand affinities of an antifluorescyl Fab (4-4-20) in two solvent systems. *Proteins* **3:** 155–160.

Hanes, J. and Plückthun, A. 1997. In vitro selection and evolution of functional proteins by using ribosome display. *Proc. Natl. Acad. Sci.* **94:** 4937–4942.

Herron, J.N., Kranz, D.M., Jameson, D.M., and Voss Jr., E.W. 1986. Thermodynamic properties of ligand binding by monoclonal anti-fluorescyl antibodies. *Biochemistry* **25:** 4602–4609.

Herron, J.N., He, X.M., Mason, M.L., Voss Jr., E.W., and Edmundson, A.B. 1989. Three-dimensional structure of a fluorescein–Fab complex crystallized in 2-methyl-2,4-pentanediol. *Proteins* **5:** 271–280.

Herron, J.N., Terry, A.H., Johnston, S., He, X.M., Guddat, L.W., Voss Jr., E.W., and Edmundson, A.B. 1994. High resolution structures of the 4-4-20 Fab-fluorescein complex in two solvent systems: Effects of solvent on structure and antigen-binding affinity. *Biophys. J.* **67:** 2167–2183.

Honegger, A. and Plückthun, A. 2001. Yet another numbering scheme for immunoglobulin variable domains: An automatic modeling and analysis tool. *J. Mol. Biol.* **309:** 657–670.

Hubbard, S.J. and Thornton, J.M. 1993. NACCESS *computer program*. University College, London, UK.

James, L.C., Roversi, P., and Tawfik, D.S. 2003. Antibody multispecificity mediated by conformational diversity. *Science* **299:** 1362–1367.

Jermutus, L., Honegger, A., Schwesinger, F., Hanes, J., and Plückthun, A. 2001. Tailoring *in vitro* evolution for protein affinity or stability. *Proc. Natl. Acad. Sci.* **98:** 75–80.

Jung, S. and Plückthun, A. 1997. Improving in vivo folding and stability of a single-chain Fv antibody fragment by loop grafting. *Prot. Eng.* **10:** 959–966.

Kabat, E.A., Wu, T.T., Perry, H.M., Gottesmann, K.S., and Foeller, C. 1991. *Sequences of proteins of immunological interest*. National Institutes of Health publication no. 91-3242, 5th ed. United States Department of Health and Human Services, Bethesda, MD.

Korndorfer, I.P., Beste, G., and Skerra, A. 2003. Crystallographic analysis of an "anticalin" with tailored specificity for fluorescein reveals high structural plasticity of the lipocalin loop region. *Proteins* **53:** 121–129.

Kranz, D.M., Herron, J.N., and Voss Jr., E.W. 1982. Mechanisms of ligand binding by monoclonal anti-fluorescyl antibodies. *J. Biol. Chem.* **257:** 6987–6995.

Krebber, C., Spada, S., Desplancq, D., and Plückthun, A. 1995. Co-selection of cognate antibody-antigen pairs by selectively-infective phages. *FEBS Lett.* **377:** 227–231.

Krebber, C., Spada, S., Desplancq, D., Krebber, A., Ge, L., and Plückthun, A. 1997. Selectively-infective phage (SIP): A mechanistic dissection of a novel in vivo selection for protein–ligand interactions. *J. Mol. Biol.* **268:** 607–618.

Kunkel, T.A., Bebenek, K., and McClary, J. 1991. Efficient site-directed mutagenesis using uracil-containing DNA. *Methods Enzymol.* **204:** 125–139.

Laskowski, R.A., Macarthur, M.W., Moss, D.S., and Thornton, J.M. 1993. Procheck—A program to check the stereochemical quality of protein structures. *J. Appl. Crystallog.* **26:** 283–291.

Lee, B. and Richards, F.M. 1971. The interpretation of protein structures: Estimation of static accessibility. *J. Mol. Biol.* **55:** 379–400.

Lim, K. and Herron, J.N. 1995. Molecular dynamics of the anti-fluorescein 4-4-20 antigen-binding fragment. 1. Computer simulations. *Biochemistry* **34:** 6962–6974.

Lim, K., Jameson, D.M., Gentry, C.A., and Herron, J.N. 1995. Molecular dynamics of the anti-fluorescein 4-4-20 antigen-binding fragment. 2. Time-resolved fluorescence spectroscopy. *Biochemistry* **34:** 6975–6984.

Matthews, B.W. 1968. Solvent content of protein crystals. *J. Mol. Biol.* **33:** 491–497.

Midelfort, K.S., Hernandez, H.H., Lippow, S.M., Tidor, B., Drennan, C.L., and Wittrup, K.D. 2004. Substantial energetic improvement with minimal structural perturbation in a high affinity mutant antibody. *J. Mol. Biol.* **343:** 685–701.

Mummert, M.E. and Voss Jr., E.W. 1996. Effects of secondary forces on the ligand binding properties and variable domain conformations of a monoclonal anti-fluorescyl antibody. *Mol. Immunol.* **33:** 1067–1077.

Navaza, J. 1990. Accurate computation of the rotation matrices. *Acta Crystallogr. A* **46:** 619–620.

———. 1994. AMoRe—An automated package for molecular replacement. *Acta Crystallogr. A* **50:** 157–163.

Navaza, J. and Saludjian, P. 1997. AMoRe: An automated molecular replacement program package. *Macromol. Crystallogr. Pt A* **276:** 581–594.

Nieba, L., Honegger, A., Krebber, C., and Plückthun, A. 1997. Disrupting the hydrophobic patches at the antibody variable/constant domain interface: Improved in vivo folding and physical characterization of an engineered scFv fragment. *Prot. Eng.* **10:** 435–444.

Omelyanenko, V.G., Jiskoot, W., and Herron, J.N. 1993. Role of electrostatic interactions in the binding of fluorescein by anti-fluorescein antibody 4-4-20. *Biochemistry* **32:** 10423–10429.

Otwinovski, Z. 1993. DENZO: Oscillation data and reducing program. In *Data collection and processing*. (eds. L. Sawyer et al.), pp. 56–63, DLSCI/R34 Daresbury Laboratory, Warrington, Cheshire, UK.

Paci, E., Caflisch, A., Plückthun, A., and Karplus, M. 2001. Forces and energetics of hapten–antibody dissociation: A biased molecular dynamics simulation study. *J. Mol. Biol.* **314:** 589–605.

Pedrazzi, G., Schwesinger, F., Honegger, A., Krebber, C., and Plückthun, A. 1997. Affinity and folding properties both influence the selection of antibodies with the selectively infective phage (SIP) methodology. *FEBS Lett.* **415:** 289–293.

Ros, R., Schwesinger, F., Anselmetti, D., Kubon, M., Schäfer, R., Plückthun, A., and Tiefenauer, L. 1998. Antigen binding forces of individually addressed single-chain Fv antibody molecules. *Proc. Natl. Acad. Sci.* **95:** 7402–7405.

Rossman, M.G. and Blow, D.M. 1962. The detection of subunits within the crystallographic asymmetric unit. *Acta Crystallogr. A* **15:** 24–31.

Roussel, A. and Cambillau, C. 1991. The Turbo-Frodo graphics package. In *Silicon graphics geometry partners directory*, p. 81. Silicon Graphics, Mountain View, CA.

Schulze-Gahmen, U., Rini, J.M., and Wilson, I.A. 1993. Detailed analysis of the free and bound conformations of an antibody. X-ray structures of Fab 17/9 and three different Fab-peptide complexes. *J. Mol. Biol.* **234:** 1098–1118.

Schwesinger, F., Ros, R., Strunz, T., Anselmetti, D., Güntherodt, H.J., Honegger, A., Jermutus, L., Tiefenauer, L., and Plückthun, A. 2000. Unbinding forces of single antibody–antigen complexes correlate with their thermal dissociation rates. *Proc. Natl. Acad. Sci.* **97:** 9972–9977.

Swindlehurst, C.A. and Voss Jr., E.W. 1991. Fluorescence measurements of immune complexes of Mab 4-4-20 with isomeric haptens. *Biophys. J.* **59:** 619–628.

Terzyan, S., Ramsland, P.A., Voss, E.W., Herron, J.N., and Edmundson, A.B. 2004. Three-dimensional structures of idiotypically related Fabs with intermediate and high affinity for fluorescein. *J. Mol. Biol.* **339:** 1141–1151.

Vaughan, T.J., Williams, A.J., Pritchard, K., Osbourn, J.K., Pope, A.R., Earnshaw, J.C., McCafferty, J., Hodits, R.A., Wilton, J., and Johnson, K.S. 1996. Human antibodies with sub-nanomolar affinities isolated from a large non-immunized phage display library. *Nat. Biotech.* **14:** 309–314.

Wallace, A.C., Laskowski, R.A., and Thornton, J.M. 1995. Ligplot—A program to generate schematic diagrams of protein ligand interactions. *Prot. Eng.* **8:** 127–134.

Whitlow, M., Howard, A.J., Wood, J.F., Voss Jr., E.W., and Hardman, K.D. 1995. 1.85 Å structure of anti-fluorescein 4-4-20 Fab. *Prot. Eng.* **8:** 749–761.